5

EMIC Waves in the Inner Magnetosphere

M. E. Usanova,[1] I. R. Mann,[2] and F. Darrouzet[3]

5.1. INTRODUCTION

Electromagnetic ion cyclotron (EMIC) waves are transverse plasma waves generated in the inner magnetosphere by ring current ions with perpendicular temperature anisotropy ($T_{perp} > T_{par}$) and are typically registered on the ground in the Pc1-2 (0.1–5 Hz) frequency range. Both theory and observations have shown that during the evolution of EMIC instability and EMIC wave growth, waves and ions exchange energy and momentum, which can lead to decreases in ion pitch angle, ion loss into the atmosphere, and isotropization of the initially unstable ion distribution [e.g., *Cornwall*, 1965; *Søraas*, *et al*., 1980; *Usanova et al*., 2010]. Interaction with EMIC waves is also believed to be a potentially important loss mechanism for radiation belt electrons, which can undergo cyclotron resonance with EMIC waves if the Doppler shifted wave frequency matches the electron gyrofrequency.

In a cold magnetospheric plasma typically consisting of H^+, He^+, and O^+ ion species, there are forbidden band gaps for EMIC wave generation and propagation around heavy ion gyrofrequencies that split the wave spectrum into multiple branches [e.g., see *Fraser*, 1985]. The dispersion relation (normalized frequency as a function of the wave number) for an EMIC wave propagating parallel to the magnetic field in a plasma consisting of H^+, He^+, and O^+ species is shown in Figure 5.1 [adapted from *Thorne et al*., 2006]. The growth rates on each branch are typically controlled by proton temperature anisotropy, ion composition, and cold plasma density [e.g., *Kozyra et al*., 1984; *Horne and Thorne*, 1997]. The energy of relativistic electrons that can interact with EMIC waves is very sensitive to the ratio of local plasma density and magnetic field strength and to the proximity of the wave frequency to ion gyrofrequencies [e.g., *Summers and Thorne*, 2003]. Also the ability of EMIC waves to scatter relativistic electrons depends on wave and plasma properties (e.g., on the wave normal angle or polarization).

Ukhorskiy et al. [2010] showed that in a cold plasma approximation, the minimum electron kinetic energy required for cyclotron resonance with EMIC waves has a singularity at the ion gyrofrequency. They demonstrated that EMIC waves could interact with the bulk of electron energy distribution (<2 MeV) only in regions of relatively high plasma density, and only if the wave frequency is sufficiently close to heavy ion gyrofrequency. Note, however, that the regions where EMIC waves are excited are not necessarily well characterized as cold plasma. In the case of a warm plasma, the characteristics of the EMIC waves, not least their frequency and wavenumber spectra, are changed significantly from that developed in a cold plasma, and consequently, this can change the energies of radiation belt electron that might be resonant with the EMIC waves [e.g., see *Silin et al*., 2011]. Nonetheless, regions such as the duskside plasmapause and its extension onto the plasmaspheric plume are hypothesized as potentially important regions for EMIC wave–MeV electron interactions (these regions are shown schematically in Figure 5.2). In this schematic (taken from *Reeves et al*. [2007], as adapted from *Summers et al*. [1998]), preferential excitation of EMIC waves along the duskside plasmapause is suggested as a possible explanation for

[1]*Laboratory for Atmospheric and Space Physics, University of Colorado at Boulder, Boulder, Colorado, USA*

[2]*Department of Physics, University of Alberta, Edmonton, Alberta, Canada*

[3]*Belgian Institute for Space Aeronomy, Brussels, Belgium*

Low-Frequency Waves in Space Plasmas, Geophysical Monograph 216, First Edition.
Edited by Andreas Keiling, Dong-Hun Lee, and Valery Nakariakov.

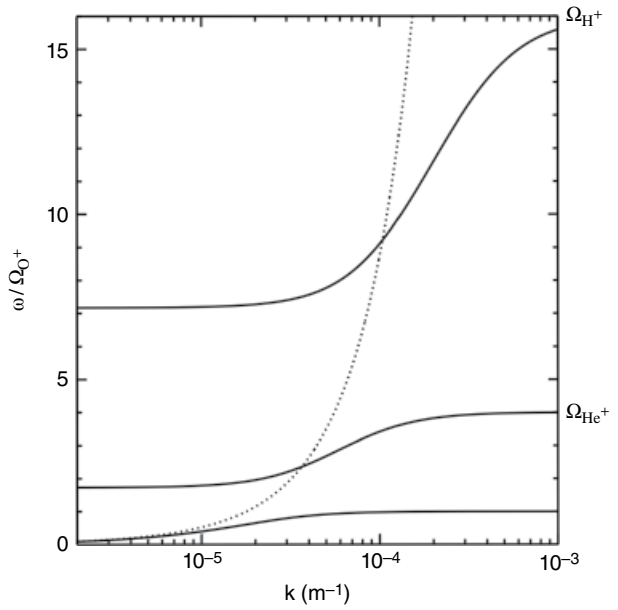

Figure 5.1 EMIC wave dispersion relation for parallel propagation in a plasma composed of 70% H^+, 20% He^+, and 10% O^+ ion species. The solid curves show the three left-hand polarized modes below the H^+, He^+, and O^+ cyclotron frequencies, respectively. The dashed curve denotes the right-hand polarized mode, which becomes important for oblique propagation. Adapted from *Thorne et al.* [2006].

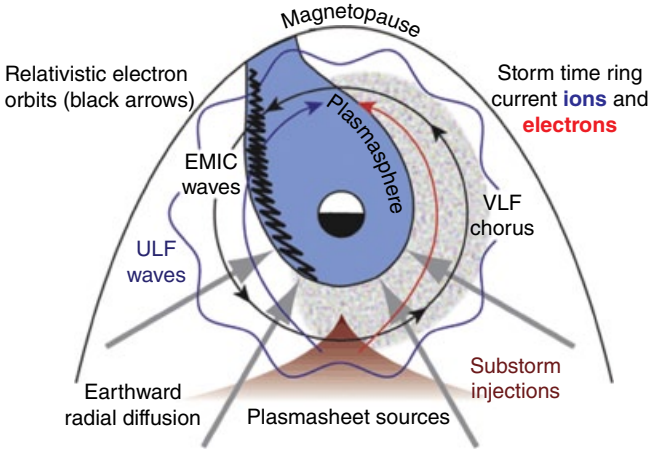

Figure 5.2 Different mode plasma waves that can interact with radiation belt electrons [schematic diagram taken from *Reeves et al.*, 2007]. EMIC waves preferentially excited along the duskside plasmapause and scattering relativistic electrons into the loss cone have been proposed as a candidate for outer radiation belt electron depletion during the main storm phase [e.g., *Summers and Thorne*, 2003].

the rapid radiation belt flux dropout that can occur during the main phase of geomagnetic storms. In this paradigm, ions injected due to enhanced storm-time magnetospheric convection from the tail adiabatically develop temperature anisotropy while they are being transported inward, drift in clockwise (westward) direction around the Earth, intersect the cold plasmapause and give rise to EMIC waves. At the same time, radiation belt electrons drifting in the counterclockwise (eastward) direction penetrate the region of EMIC activity from the opposite side and may get pitch angle scattered by the EMIC waves into the atmosphere.

However, there are important potential problems and inconsistencies between the paradigm represented in the schematic in Figure 5.2 and EMIC wave observations. For example, there has been very limited direct experimental evidence supporting the hypothesis that EMIC waves scatter the core population of radiation belt electrons into the loss cone [e.g., *Miyoshi et al.*, 2008], and in very recent work it has been shown that this scattering may only be significant for low-pitch angle part of the electron distribution, even at ultra-relativistic energies where such EMIC wave interactions most easily occur [*Usanova et al.*, 2014; *Kersten et al.*, 2014]. Based in such observations, it seems unlikely that EMIC waves alone can scatter the core of the electron distribution into the loss cone; rather, more likely EMIC waves are not typically responsible for the radiation belt electron dropouts observed during the main phase of magnetic storms [*Usanova et al.*, 2014].

The relationship between EMIC wave occurrence and enhanced plasma densities, as well as EMIC wave prevalence during a storm's main phase, still remains controversial. For example, statistical storm-time observations of EMIC waves at geosynchronous orbit presented by *Fraser et al.* [2010] showed that only 29% of their EMIC events were observed during a storm's main phase. Similarly, ground-based observations often show a pronounced lack of EMIC activity in the main phase of magnetic storms. For example, statistical studies by *Engebretson et al.* [2008a, b] using both ground-based and *in situ* observations did not support the hypothesis that EMIC waves were dominant during storm main phase. An illustration of this behavior is presented in Figure 5.3, which shows ground-based EMIC wave observations in the inner magnetosphere (from a station at $L = 4.23$) through the progression of a magnetic storm. During the main phase in the period of minimum Dst there is a broadband wave activity in the Pc1 band, which is typical for disturbed conditions; however, there is no evidence for EMIC wave emissions. EMIC waves only start later in the storm, during the period of rising Dst. In contrast, an increased occurrence of waves that was observed by the CRRES satellite *in situ* at $L < 7$ during disturbed conditions in the local time sector from pre-noon to dusk (10 h ≤ MLT < 19 h) was discussed by *Keika et al.* [2013], for example, as likely related to enhanced cold plasma densities in this local time sector.

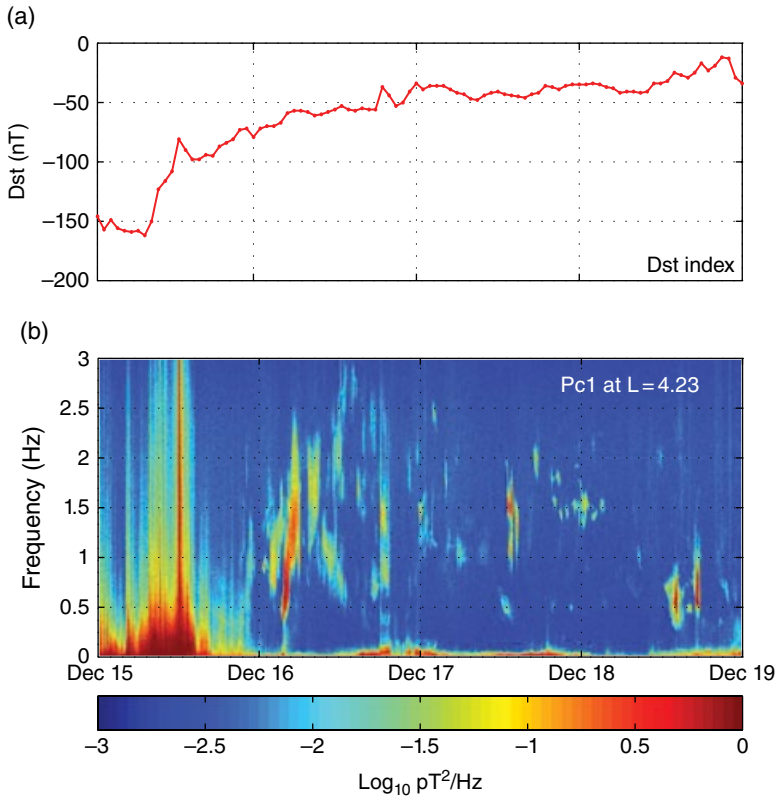

Figure 5.3 EMIC Pc1 waves as observed from the ground in the recovery phase of a geomagnetic storm with minimum Dst on December 15, 2006. (a) storm-time disturbance (Dst) index between December 15 and December 19, 2006. (b) Spectrogram of the H-component of the magnetic field observed on the ground by the Parksite station (Canada) at $L = 4.23$.

In relation to the spatial localization of EMIC wave activity, there have been several statistical studies, in particular, by *Anderson et al.* [1992], *Usanova et al.* [2012], and *Keika et al.* [2013], demonstrating that EMIC wave occurrence in the inner magnetosphere is low, and that the waves have a much higher occurrence rate at higher *L*-shells, closer to the magnetopause. Consistent with these studies, *Usanova et al.* [2013] found that the occurrence rate of EMIC waves inside plasmaspheric plumes observed by the Cluster satellite is also small (~10%) and increases with *L*-shell, with EMIC wave occurrence being more strongly controlled by solar wind dynamic pressure than enhanced plasma density inside plasmaspheric plumes. In this chapter, we will further investigate EMIC wave occurrence and extend the analysis of *Usanova et al.* [2013] to include a Cluster survey of plasmapause crossings in a similar manner. We also found rather low EMIC wave occurrence rates even in the vicinity of the plasmapause (about 8%).

Nevertheless, despite low EMIC wave occurrence in the inner magnetosphere, some works such those by *Turner et al.* [2013] and *Sakaguchi et al.* [2013] continue to suggest that EMIC waves might be responsible for radiation belt losses. Therefore, the relative importance of EMIC waves in the dynamics of the radiation belts remains an unresolved problem, and their properties, especially in the inner magnetosphere, need further experimental and theoretical examination.

5.2. EMIC WAVE GENERATION AND PROPAGATION TO THE GROUND

In the inner magnetosphere, EMIC waves are thought to be preferentially excited in the equatorial region [*Mauk*, 1982] where the background magnetic field reaches its minimum, and where the anisotropy and phase space density of energetic ion distributions that provide the energy source for EMIC instability are usually maximim. Using wave Poynting vector measurements onboard the CRRES satellite, *Loto'aniu et al.* [2005] showed that the source region is typically confined within ±11° of the magnetic equator. At higher *L*-shells in the dayside magnetosphere, the region of minimum magnetic field and hence, the wave source can move away from the magnetic equator [e.g., *McCollough et al.*, 2010; *Liu et al.*, 2012]. In the generation region, EMIC waves are typically elliptically polarized in

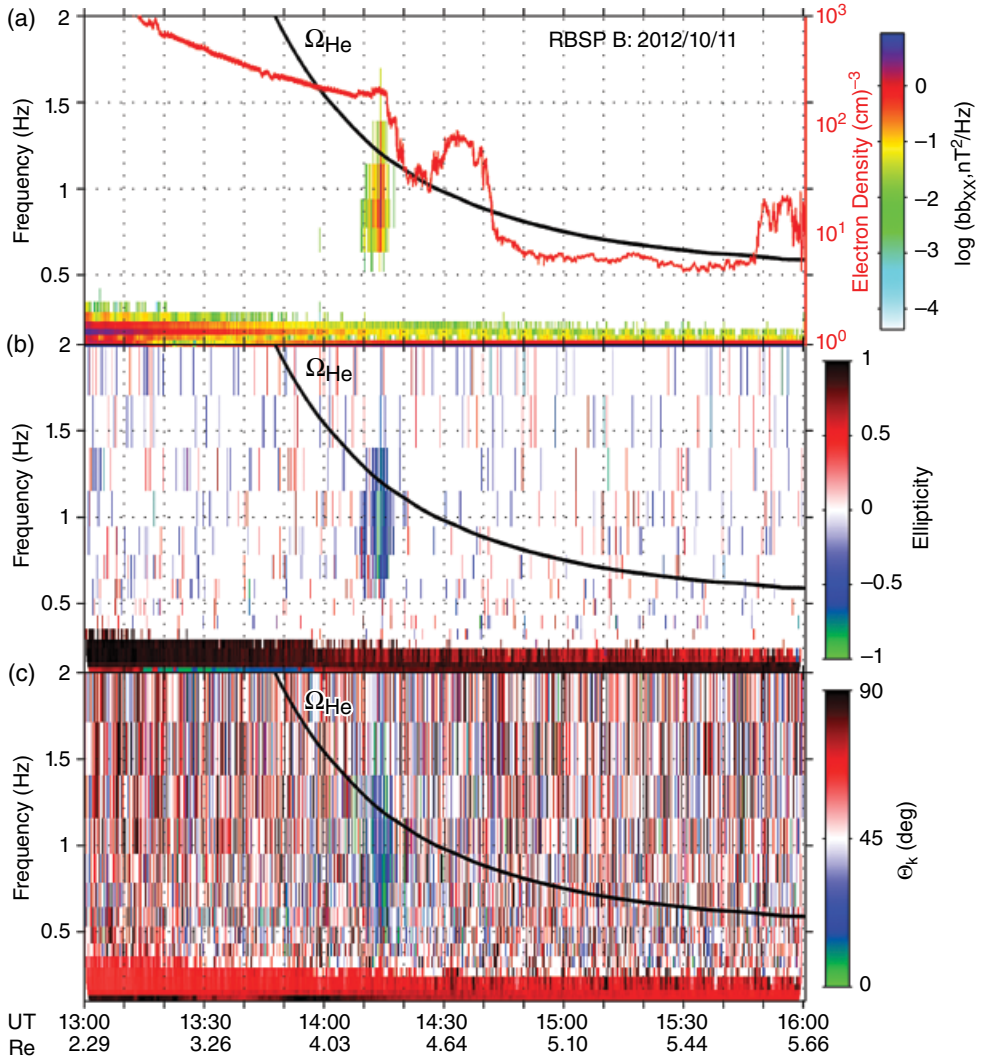

Figure 5.4 EMIC wave properties observed by Van Allen Probe B on October 11, 2012. (a) wavelet-transformed magnetic field power spectral density with the background electron density derived from the spacecraft potential over-plotted on top (red line); (b) ellipticity (green—left-hand; dark red—right-hand); (c) wave normal angle (green—parallel to the background magnetic field; dark red—perpendicular to the background magnetic field). The black lines show the local helium gyrofrequency.

a left-handed sense, which corresponds to the direction of ion gyration around the magnetic field, and propagate almost parallel to the background magnetic field. Consistent with the observations of *Loto'aniu et al.* [2005], an example of an EMIC wave observed in the equatorial inner magnetosphere (L~4) from October 11, 2012, on Van Allen Probe B is shown in Figure 5.4. This figure shows an EMIC wave emission in the helium band (spectral power below the local helium gyrofrequency, Figure 5.4a), with left-handed polarization (negative ellipticity, Figure 5.4b), propagating obliquely to the background magnetic field (as shown in the wave normal angle in Figure 5.4c). Following their generation in the equatorial region, EMIC waves can propagate along the magnetic field line all the way to the ionosphere and then also be detected by magnetometers on the ground. EMIC growth typically maximizes for wave propagation parallel to the background magnetic field, but although the waves remain field guided, they can become oblique, especially as the waves propagate toward the ionosphere (e.g., [*de Soria-Santacruz et al.*, 2013], and references therein). Similarly, ducting of ray paths can result in the guiding of waves along the direction of the background magnetic field, and the ducting can occur in density structures close to the plasmapause or in plasmaspheric plumes (e.g., Figure 2a of *de Soria-Santacruz et al.* [2013], and

references therein). During this propagation, the wave can exhibit changes in its properties, for example, changes in polarization from left- to right-handed due to interaction with the nonuniform ambient plasma between the magnetosphere and ionosphere. As mentioned in Section 5.1, minor ions (helium and oxygen) can split the wave spectrum into three bands, which can be observed simultaneously or separately. Sometimes the oxygen band waves have frequencies that overlap with other broadband low-frequency waves in the same band, and this can make the oxygen band emissions hard to identify. In the equatorial plane, both hydrogen band and helium band waves can be observed, and as shown in the statistics presented by *Keika et al*. [2013], the hydrogen band emissions can occur in the local afternoon during all geomagnetic conditions, and also be seen in the local morning when active. In contrast, the helium band waves are dominant near noon and in the afternoon, can be seen on lower *L*-shells during active times. Consequently, as might be expected based on the *Keika et al*. [2013] statistics, the hydrogen band can often be seen *in situ* in combination with emissions in the helium band. For example, the spectrograms in Figures 5.5b and 5.5d from the geosynchronous GOES satellite magnetic field measurements show clear emissions both above and below the local helium gyrofrequency.

The presence of helium ions in the magnetosphere is thought to prevent EMIC waves in the hydrogen band from propagating to the ground [*Rauch et al*., 1982] due to H^+-He^+ bi-ion resonance, which they can encounter when their frequency equals $\frac{(1+3\eta)F^+_{He}}{(1+0.75\eta)}$, where η is the fraction of He^+ ions [*Roux et al*., 1992]. Consistent with this theory, the conjugate ground-satellite EMIC wave study by *Usanova et al*. [2008] showed that while waves in both the helium and the hydrogen bands were observed *in situ*, only the helium band propagated to the ground. However, if the fraction of He^+ ions is less than a few percent, hydrogen band waves are believed to be able to tunnel through this resonance frequency and reach the ionosphere [*Perraut et al*., 1984; *Anderson et al*., 1996; *Johnson and Cheng*, 1999]. Conjugate ground-satellite observations have shown that, on average, the hydrogen band is observed on the ground in ~50% cases, with the wave transmission coefficient being strongly dependent on the wave frequency for a given fraction of He^+ ions [*Perraut et al*., 1984]. In the example shown in Figure 5.5, GOES 13 equatorial EMIC wave observations from L = 6.8 clearly demonstrate coincidental EMIC wave emissions in both bands (Figure 5.5b). However, although not precisely conjugate, the ground observations from the CARISMA array of fluxgate magnetometers [*Mann et al*., 2008], in particular, from the Rabbit Lake station (RABB) at the footprint of an L = 6.6 field line west of GOES13, show EMIC activity predominately in the helium band (Figure 5.5e). Further west, the observations from GOES 15 are approximately conjugate to the Fort Smith (FSMI station; see the map in Figure 5.5c). Although the GOES15 data are mostly characterized as emissions below the local helium gyrofrequency, the emission at around 03:30 UT, which is clearly in the hydrogen band, has no counterpart on the ground at FSMI. Even this single example demonstrates the complexity and structure of EMIC wave observations both on the ground and in space, even when such conjugate observations are made on the same *L*-shell and in the same magnetic local time (MLT) sector.

Multiband structures that are commonly observed in EMIC emissions seen on the ground [e.g., *Fukinishi et al*., 1981] also need not necessarily be related to a single multiband generation region in the magnetospheric source region. Such multiple-band ground observations may also result from waves with different frequencies being ducted from multiple sources at different *L*-shells and local times in the magnetosphere to the station location on the ground [e.g., *Greifinger and Greifinger*, 1968], with selective transmission of incident wave frequencies through the ionospheric Alfvén resonator (IAR) also probably playing an important role [*Kerttula* et al., 2001; *Prikner et al*., 2004]. Wave ducting in the ionospheric waveguide will be addressed in more detail in Section 5.4.

Theoretical studies [e.g., *Horne and Thorne*, 1993] have identified the plasmapause as a preferred location for EMIC wave excitation. This preference is explained by the fact that the convective wave growth, which is inversely proportional to the Alfvén speed, maximizes just inside the plasmapause, in the region where cold plasma density is relatively high and the background magnetic field is relatively low. Also the steep plasma density gradient at the plasmapause can guide waves by keeping the wave normal angle small and hence aid wave growth over consecutive passages as they propagate through the equatorial source region. More recent EMIC wave growth and propagation analysis by *Chen et al*. [2009], who used a ray tracing technique, showed that the maximum wave gain should be observed just inside the plasmapause, in the plasmaspheric plumes, as well as in the low-density trough at high *L*-shells.

Observational case studies [e.g., *Usanova et al*., 2008, 2014; *Liu et al*., 2013] have provided evidence in support of the hypothesis that the plasmapause can generate conditions favorable for wave trapping in radially narrow ducts. Figure 5.4 shows observations of EMIC waves in the equatorial magnetosphere by the Van Allen Probes as were generated in a radially narrow region, just inside the plasmapause, and propagated at wave normal angles ~10–20° with respect to the background magnetic field and with left-handed polarization rotation (negative ellipticity).

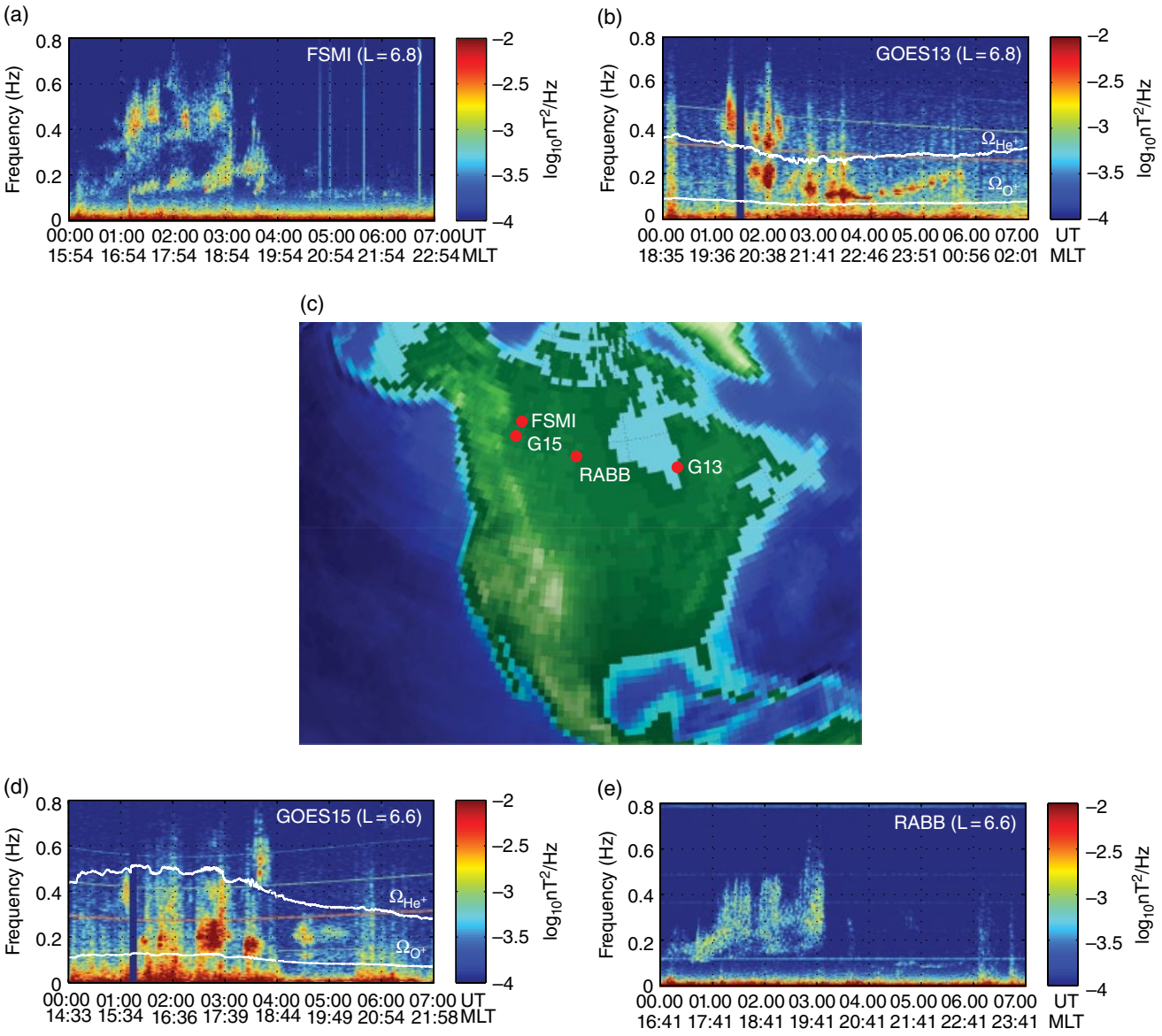

Figure 5.5 Ground and space observations of the helium and hydrogen band EMIC waves on January 17, 2013. (a) EMIC waves are observed on the ground at Fort Smith (FSMI) and closely magnetically conjugate in the equatorial plane at the geosynchronous GOES 15 satellite (d), as well as further east at the geosynchronous GOES 13 satellite (b) and at a longitude in between on the ground, at Rabbit Lake (RABB) (e). White lines in (b, d) denote the local He^+ and O^+ gyrofrequencies. The map in (c) shows the magnetic ground footprints of GOES 13, GOES 15, and the locations of the Fort Smith (L = 6.8) and Rabbit Lake (L = 6.6) stations.

5.3. EMIC WAVES CLOSE TO THE PLASMAPAUSE: STATISTICS

Interestingly, despite the results from numerous case studies that show an association of EMIC waves with the plasmapause, in statistical studies the plasmapause has not been found to be an especially preferred location for EMIC wave generation [*Fraser and Nguyen*, 2001]. Surveys of the wave occurrence from multiple satellite missions show that EMIC wave probability peaks in the duskside magnetosphere and increases with radial distance [e.g., *Anderson et al.*, 1992; *Usanova et al.*, 2012; *Keika et al.*, 2013]. In this section, we examine the relationship between EMIC wave occurrence and plasmapause location using a statistical survey of 148 inbound plasmasphere transits by the Cluster spacecraft [*Darrouzet et al.*, 2013]. This dataset is

particularly important as *Darrouzet et al*. [2013] also looked at the location of the electron radiation belt boundaries with respect to the plasmapause, and there they found that during prolonged quiet conditions the plasmapause was co-located with the outer boundary of the outer radiation belt and moved closer to the inner boundary during disturbed conditions. This observation could be especially interesting in relation to EMIC wave interactions with radiation belt electrons if EMIC waves were observed in the vicinity of the plasmapause during disturbed conditions. Consequently in this section we examine the relationship between EMIC wave occurrence and these plasmapause crossings from the *Darrouzet et al*. [2013] database.

Darrouzet et al. [2013] identified the plasmapause crossings by Cluster 3 between 2007 and 2009 (an interval of predominately quiet geomagnetic conditions) when Cluster perigee was close to 2 R_E. They used the WHISPER (Waves of HIgh frequency and Sounder for Probing of Electron density by Relaxation) instrument that measures high-frequency electric fields and thus derived electron plasma density from electron plasma frequency [*Decreau et al*., 2001; *Darrouzet et al*., 2009]. The plasmapause was identified based on a density increase of at least a factor of 3 over an L-distance of 0.5 R_E or less, with an increase up to a density larger than 20 cm^{-3}. Plasmapause crossings covered all MLT sectors uniformly, except the early morning, where the probability of plasmapause detection was close to zero.

Using an automated Pc1 detection algorithm [*Bortnik et al*., 2007], we further identified EMIC waves from magnetic field measurements by the Cluster fluxgate magnetometer (FGM) in the vicinity of the plasmapause and investigated the relationship between EMIC wave occurrence and the plasmapause location—similar to the approach of *Usanova et al*. [2013] who analyzed EMIC wave occurrence in plasmaspheric plumes. We used magnetic field data in a field-aligned coordinate system within an hour window centered on a plasmapause crossing. To these data, we applied the *Bortnik et al*. [2007] automated wave detection algorithm that Fast Fourier Transform (FFT) time series into frequency-time spectral matrices and selects spectral peaks that stand out (at least one magnitude greater in spectral power) above the background noise. The algorithm returns three recorded frequencies: a bottom frequency, a top frequency, and a frequency of maximum power, as are shown in Figure 5.6 superposed over spectrograms of the perpendicular magnetic field component in the field-aligned coordinate system. The black and the purple dots in this figure define the EMIC bandwidth and the maximum power, respectively, determined by the algorithm. Figure 5.6 also shows the EMIC wave location with respect to the plasmapause: Figure 5.6a shows an example of emissions from just inside the plasmapause, and Figure 5.6b, an example with EMIC waves both inside and outside and the plasmapause and separated by a radial gap. In each figure, the white vertical bars denote the plasmapause.

EMIC waves were observed during 26 (18%) out of 148 plasmapause crossings (see the diagram in Figure 5.7): 15 (10%) outside at high L-shells, 6 (4%) just inside, 3 (2%)

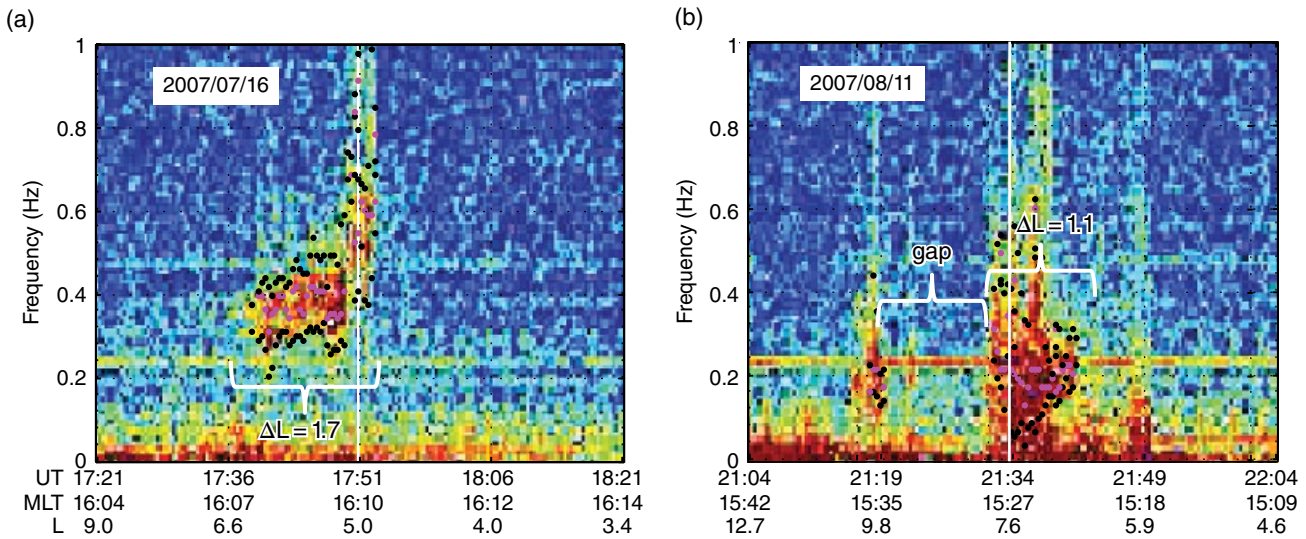

Figure 5.6 EMIC wave location with respect to the plasmapause as observed by Cluster 3. (a) Example of narrow emission of width 1.7 R_E just outside the plasmapause on July 16, 2007; (b) two narrow and distinct EMIC wave bursts separated by a gap of 2.2 R_E located well outside, and just inside the plasmapause, on August 11, 2007. In each panel the white vertical line shows the plasmapause location, and the black and the purple dots define the EMIC bandwidth and the frequency of maximum power, respectively, derived using the *Bortnik et al*. [2007] technique.

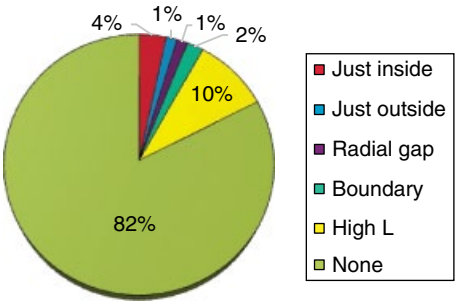

Figure 5.7 EMIC wave event occurrence in the plasmapause vicinity based on the Cluster plasmapause crossing survey completed by *Darrouzet et al.* [2013].

at the plasmapause, 1 (<1%) just outside, and 1 (<1%) where two regions of EMIC emissions were observed inside and outside the plasmapause and separated by a radial gap (Figure 5.6b). Overall, EMIC waves were observed during 8% of the Cluster satellite crossings in the vicinity of the plasmapause, and their occurrence probability increased with *L*-shell, consistent with earlier observations on AMPTE/CCE [*Anderson et al.*, 1992; *Keika et al.*, 2013], THEMIS [*Usanova et al.*, 2012], and Cluster [*Usanova et al.*, 2013]. When observed in the vicinity of the plasmapause, EMIC waves tend to appear more often just inside the plasmapause and in the dusk-side MLT sector, the radial confinement of these wave emission regions being less than 1 R_E. However, none of these 26 events was observed in the storm main phase and only four during the recovery phase, in agreement with, for example, *Bortnik et al.* [2008] and *Fraser et al.* [2010], who found that EMIC waves are more typical in the storm recovery phase.

Observations of two localized EMIC wave emission regions, separated by a gap, such as shown in Figure 5.6b, have been seen before, for example, as reported by *Anderson et al.* [1992]. *Anderson et al.* [1992] noted that such events statistically were most often observed between L = 5–6, explaining this feature by a combined effect of cold background plasma density and magnetic field in producing two regions of EMIC wave amplification. Enhanced cold plasma density increases EMIC wave growth, while enhanced background magnetic field suppresses it, which makes the growth rate increase with radial distance from the Earth. At the steep plasmapause the growth rate can reach a local minimum, which results in an absence of waves just outside the plasmapause. However, this effect will not be observed if the plasmapause is broad and highly structured, as is more usually the case—consistent with only one event from our survey being detected just outside the plasmapause.

5.4. EMIC WAVE DUCTING IN THE IONOSPHERE

When EMIC waves reach low altitudes, some of their energy is transmitted to the ionosphere, undergoes mode conversion, and propagates further in the ionospheric duct in the form of right-hand polarized compressional waves [e.g., *Fraser*, 1975; *Kim et al.*, 2011], similar to seismic waves propagating from the epicenter. Due to this secondary compressional wave propagation, EMIC signatures may be detected on the ground thousands of kilometers away from the wave incident region. According to different studies, the estimate of the wave attenuation in the ionosphere varies by two orders of magnitude from 1 to 8 dB/1000 km [*Manchester et al.*, 1970] to 100 dB/1000 km [*Hayashi et al.*, 1981]. *Kim et al.* [2011] showed that the wave power attenuation increases with increasing frequency. In addition to wave power, wave polarization can provide information about the wave source location. A number of early studies [e.g., *Fraser*, 1975; *Hayashi et al.*, 1981] demonstrated that EMIC wave polarization changes gradually from left-hand polarized close to the ionospheric footprint of the source region to right-hand polarized as the wave propagates away from the injection region.

Mann et al. [2014], using data from induction coil magnetometers in the North American sector in conjunction with the Van Allen Probes, examined the relationship between the injected magnetospheric EMIC waves and the response observed in the Earth-ionosphere waveguide. They compared EMIC wave observations to simulation of wave propagation in the ionospheric duct by *Woodroffe and Lysak* [2012] and presented evidence that EMIC waves in the inner magnetosphere are confined to very narrow *L*-shell regions that are observed both in space and on the ground.

Figure 5.8a (adapted from Figure 3 in *Mann et al.* [2014]) shows the results from a polarization analysis applied to the magnetometer data (filtered between 0.83 and 1.25 Hz) in Canada and Alaska at 14:00:15–14:00:25 UT on October 11, 2012. Ten minutes after the selected interval, Van Allen Probe B saw a clear EMIC wave emission (considered above and shown in Figure 5.4) at $L \sim 4$ in the magnetosphere, conjugate to the westernmost stations. The overall structure of wave polarization and hodogram orientation remained quite stable during a ~20 min interval centered on the observation on the Van Allen Probe B. For comparison, Figure 5.8b shows the output from a simulation of the ducting of an incident EMIC wave into the ionosphere adapted from *Woodroffe and Lysak* [2012] as a function of *L*-shell and MLT. Figure 5.9 shows dynamic spectrograms of the D-component power (Figure 5.9a) and ellipticity in the horizontal plane (Figure 5.9b) on the ground, the individual spectrograms being ordered in the plot based on their relative geomagnetic latitude and longitude. Comparison between both

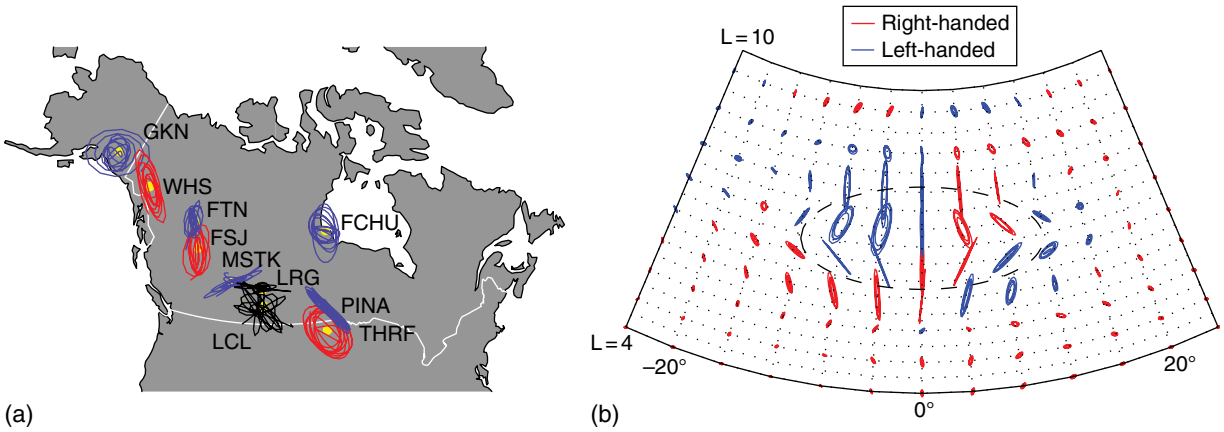

Figure 5.8 (a) Map showing the locations of CARISMA and STEP magnetometer stations observing EMIC wave activity and wave ellipticity hodograms, observed during the period of maximum EMIC wave amplitude on October 11, 2012. (b) Model results of the amplitude and polarization of EMIC waves ducted in the Earth-ionosphere waveguide (adapted from *Woodroffe and Lysak* [2012]). Left-hand polarization is shown in blue, right-hand polarization in red, and mixed or polarization in black. Adapted from *Mann et al.* [2014].

the frequency content and structuring of the EMIC waves and the polarization patterns seen on the ground suggests that there might be two strong longitudinally localized sources of EMIC waves—one close to Fort St. John (FSJ) and the other close to Pinawa (PINA), Canada. Indeed, as seen in the *Woodroffe and Lysak* [2012] modeling (Figure 5.8b), there can be sharp changes in both polarization (from left-handed to right-handed, and vice versa) at the edges of EMIC waves injection regions. This is also consistent with earlier modeling suggesting that under the source region, the waves on the ground may adopt polarization indicative of that in the magnetospheric source, while further away the polarization can rotate due to the effects of propagation in the ionospheric waveguide.

5.5. COMPARISON OF GROUND AND SPACE OCCURRENCE RATES

In order to look at how the wave propagation and its transmission through the ionosphere affect ground observations, we compared EMIC wave occurrence distributions on the ground and *in situ*. Our analysis was performed for the interval from 2007 to 2011 that is characterized by predominately quiet geomagnetic conditions. We used CARISMA FGM data along the Churchill meridional line (between L = 3.58 and 7.44) and identified EMIC waves using the same automated algorithm by *Bortnik et al.* [2007] as in Section 5.3. This auto-detection algorithm was also implemented on the THEMIS FGM data for the same five-year interval such that the occurrence rates of EMIC waves observed on the ground and in space could be compared (for more details see *Usanova et al.* [2012], and references therein). Normalized (by the total measurement time) EMIC wave occurrence as a function of L and MLT from both data sets is shown in Figures 5.10 and 5.11. THEMIS distributions (Figure 5.10a adapted from *Usanova et al.* [2012]) show that quiet-time EMIC activity is typically a dayside outer magnetosphere phenomenon, and that the EMIC occurrence rate increases toward the magnetopause, which is consistent with earlier observations by *Anderson et al.* [1992], *Fraser and Nguyen* [2001], and *Denton et al.* [2002]. Overall, the midnight sector, as seen from both the ground and space, has the lowest occurrence independent of L. At the same time, there are some differences in the ground and space occurrence pattern. In particular, the ground-based survey (Figure 5.10b) shows that EMIC wave occurrence increases with L between L = 3.58 and 6.15, and the station at highest L (FCHU; L = 7.44) has lower occurrence rates at nearly all local times. This can be due to the fact that strong auroral precipitation tends to mask EMIC waves at auroral zone stations, and during active times ducting from lower L-shells can be disrupted. At highest L-shell, the occurrence peaks in the post-noon sector, both in space and on the ground, consistent with *Posch et al.* [2010]. Interestingly, the mid-latitude ground stations (mapped to $L \sim 4$–6) demonstrate that there is a significant pre-noon population present, while the THEMIS occurrence generally peaks in the post-noon sector. Detailed comparison between the THEMIS and CARISMA EMIC occurrence rate for the Churchill line stations (same as in Figure 5.10) and corresponding L-shell on THEMIS as a function of MLT is shown in Figure 5.11. Overall, the ground probability of EMIC wave observation is low, less than 1% and by ~4 times lower than in *in situ* observations. This low ground EMIC wave occurrence

could be explained by relatively low fluxgate magnetometer sensitivity in relation to the size of the EMIC wave signal that reaches the ground, perhaps meaning that only high-amplitude waves will be detected, and this could be compounded by the potential for broadband magnetic noise on the ground (e.g., generated by ionospheric currents) acting to partially mask EMIC wave detection on the ground. However, the MLT shift in

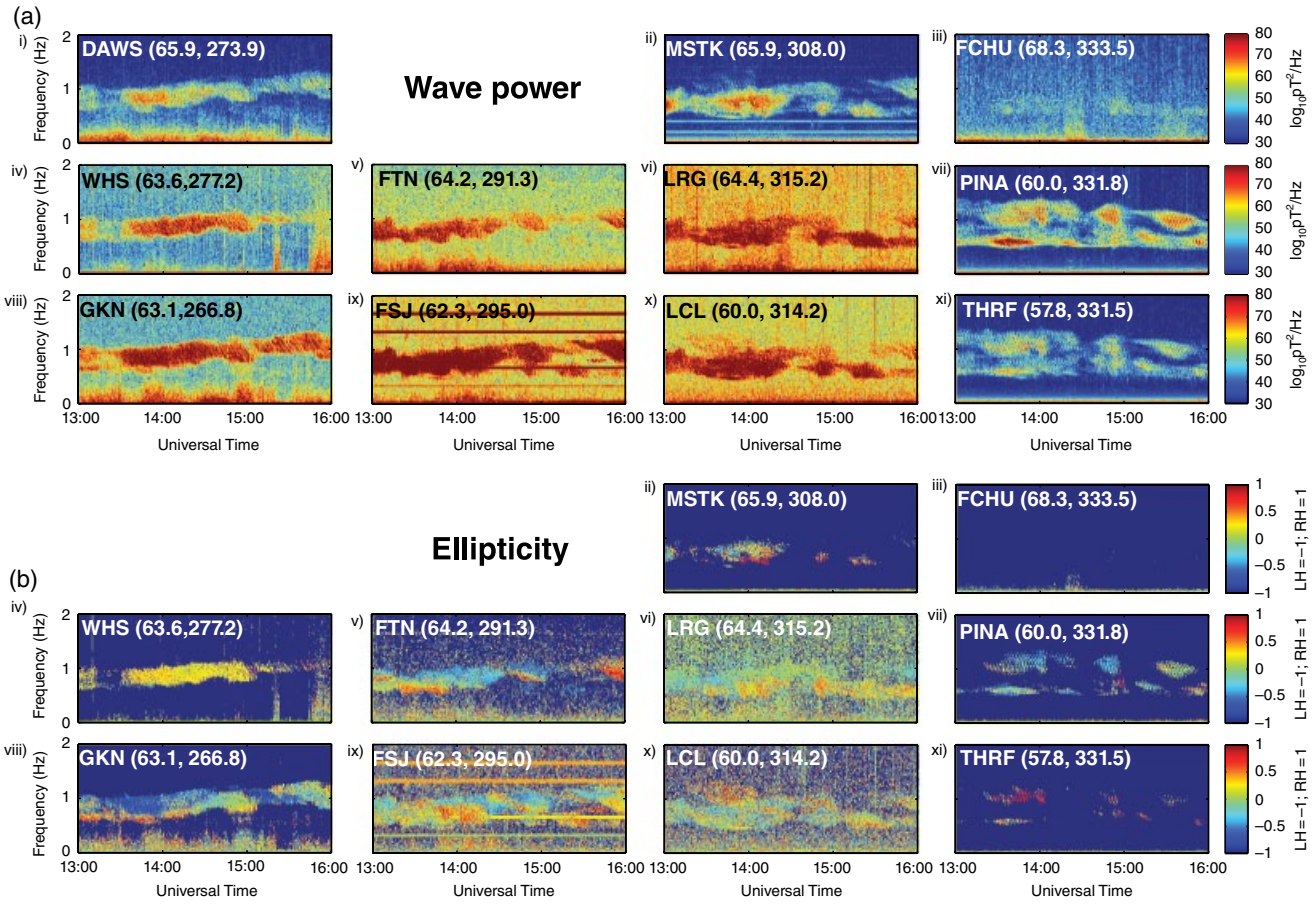

Figure 5.9 Spectrograms of the D-component (geomagnetic East–West) magnetic field power (a), and horizontal ellipticity (b), from selected CARISMA and STEP ground-based induction coil magnetometer stations between 13:00–16:00 UT on October 11, 2012. Note that no H-component data is available for DAWS, such that a polarization spectrogram cannot be computed during this interval. From Figure 4 in *Mann et al*. [2014].

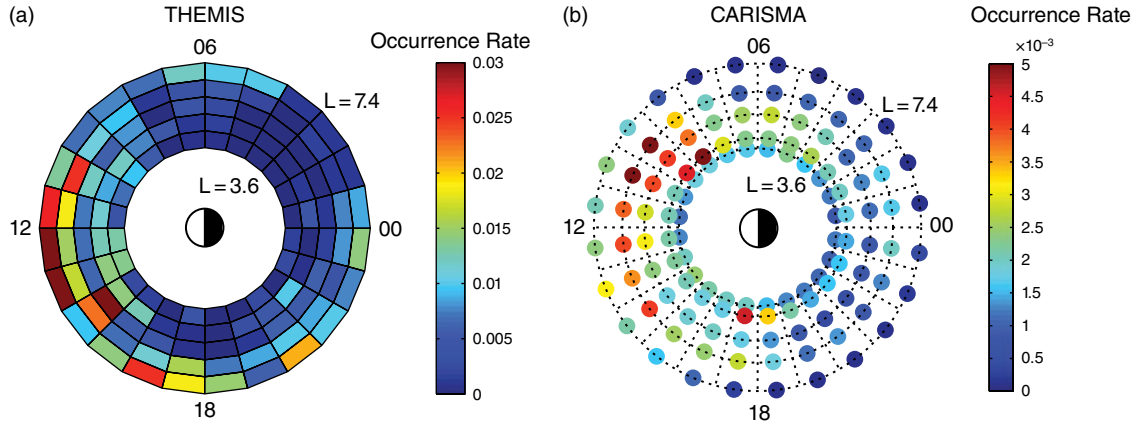

Figure 5.10 L-MLT EMIC wave occurrence for L = 3.6–7.4 between 2007–2011 determined from (a) *in situ* observations on the THEMIS satellites; and (b) ground-based CARISMA fluxgate magnetometers along the Churchill meridional line (stations located at L = 3.58, 4.06, 5.15, 6.15, and 7.44). Adapted from *Usanova et al*. [2012].

maximum wave occurrence between the ground and space is not likely to be explained by a difference between the wave amplitude on the ground and in space, as most high-amplitude EMIC waves are observed in the duskside magnetosphere [*Meredith et al.*, 2014]. Note, however, that the CRRES data used by *Meredith et al.* [2014] had little orbital coverage 09 and 13 MLT. In fact, the ground MLT distribution shown here in Figures 5.10 and 5.11 is rather consistent with earlier studies [e.g., see *Kerttula et al.*, 2001 and references therein] showing that the maximum of EMIC activity on the ground is centered on the late morning/noon sector with smaller occurrence in the afternoon. *Kerttula et al.* [2001] explained this MLT dependence, as well as the low wave incidence at high *L*-shells on the ground, by varying ionospheric transmission properties due to interaction with the IAR. Since ground EMIC waves and discrete signatures of the wave emissions structured by the natural harmonic frequencies of the IAR are only sometimes observed simultaneously, with the IAR usually only seen most often in the dusk–midnight local time sector on the ground, it is difficult to establish if this mechanism actually operates, and further analysis is certainly warranted. Also interestingly, some bins in Figure 5.11 show higher occurrence on the ground than in space, which can be due to wave ducting from other *L*-MLT sectors to the station location.

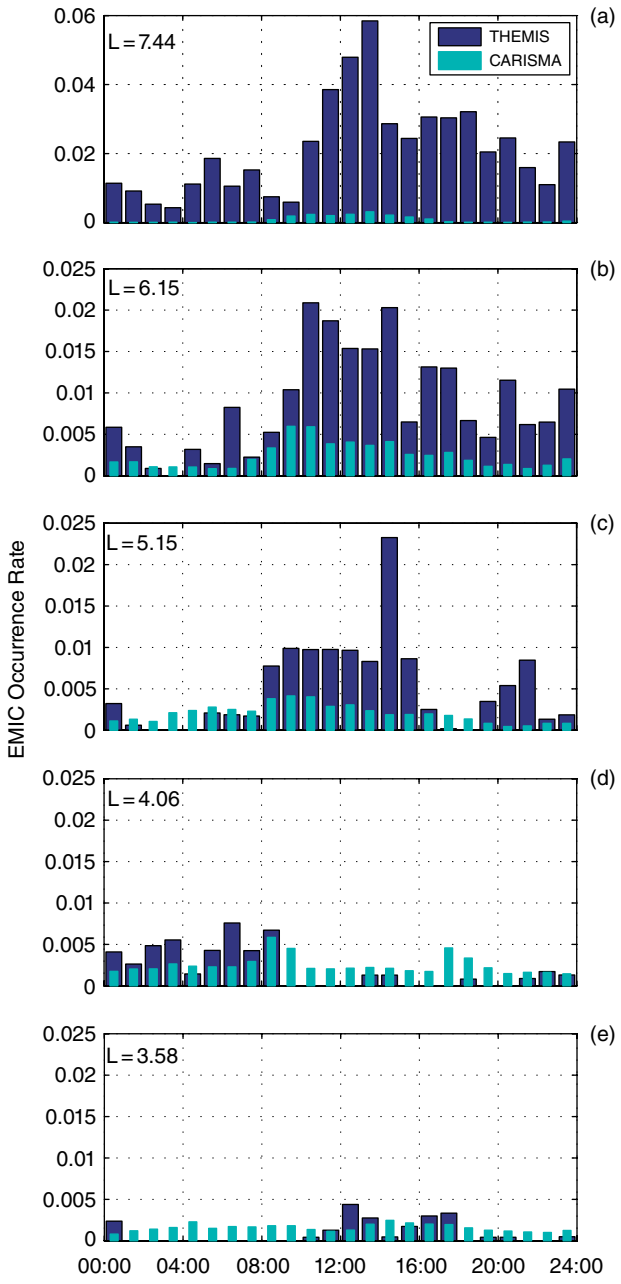

Figure 5.11 Comparison between the THEMIS and CARISMA EMIC occurrence rate for the Churchill line stations (same as in Figure 5.10) and corresponding *L*-shell on THEMIS as a function of MLT. (Note the different *y*-axis limit in panel a.)

5.6. SUMMARY AND CONCLUSIONS

In this chapter, we considered the characteristics of EMIC waves that may be important for understanding their impacts on ring current and radiation belt dynamics. We examined wave characteristics in the source region, and considered the effect of plasma composition on the wave spectrum and propagation to the ground. We also outlined the potential importance of the plasmapause for wave growth and ducting. We showed that EMIC wave activity is often observed to be generated in radially narrow regions, just inside the plasmapause, which we confirmed using both *in situ* and ground-based observations. Interestingly, analysis of satellite plasmapause crossings demonstrated that, from a statistical perspective, EMIC waves observed in the vicinity of the plasmapause have relatively low occurrence rates and are observed in lower than 10% of cases.

Ground magnetometer arrays provide continuous temporal measurements of EMIC activity and are perfect for identifying the MLT extent of wave activity in the inner magnetosphere. However, mode conversion of EMIC waves in the ionosphere and their further propagation in the ionospheric duct significantly changes EMIC wave properties, and makes it challenging to identify the EMIC wave source location from the ground. Since ground polarization from a single station exhibits variations that can be a superposition of changes in the magnetospheric source and in the ionosphere due to wave propagation and ducting, measurements from multiple stations in a magnetometer array are critical for identifying the location of the wave source from the ground. Comparison between ground and satellite statistics shows significant differences in wave distributions in space and on the ground—in particular, the shift in the wave maximum occurrence from the duskside to the morning side, as well as the relatively low occurrence of ground EMIC wave activity beyond about the GEO orbit. The differences in the spatial distributions, and absolute values, of the rates of occurrence on the ground and in space, as well as their variations with level of geomagnetic activity and

storm phase are obvious, yet a detailed explanation for these differences remains elusive and is worthy of further study.

Overall, in the recent few decades, there has been significant progress in understanding the characteristics and generation mechanism of EMIC waves. However, there are still many open questions related to their interaction with energetic particles in the inner magnetosphere. Specifically, their importance for outer radiation belt electron loss processes is yet to be fully understood.

ACKNOWLEDGMENTS

We wish to thank the Cluster WHISPER and FGM teams for the electron density and magnetic field data. We also would like to thank CDAWeb, SSCWeb, and Kyoto observatory for the use of their resources. MEU would like to thank Yuri Khotyaintsev for the wavelet transformation and wave analysis routine. MEU is supported by NASA award NAS5-01072. IRM is supported by a Discovery Grant from Canadian NSERC. We thank D. K. Milling and A. Kale for assistance with CARISMA data; CARISMA is operated by the University of Alberta, funded by the Canadian Space Agency. (Monitoring, Analyzing and Assessing Radiation Belt Loss and Energization) consortium. MAARBLE has received funding from the European Community's Seventh Framework Programme (FP7-SPACE-2010-1, SP1 Cooperation, Collaborative project) under grant agreement n° 284520. This chapter reflects only the authors' views, and the Union is not liable for any use that may be made of the information contained herein. FD thanks ESA for the Cluster mission and the Belgian Federal Science Policy Office (Belspo) through a Prodex project (contract 13127/98/NL/VJ). FD acknowledges BISA (Belgian Institute for Space Aeronomy) for its support.

REFERENCES

Anderson, B. J., et al. (1992), A statistical study of Pc 1–2 magnetic pulsations in the equatorial magnetosphere: 2. Wave properties, *J. Geophys. Res.*, *97*(A3), 3089–3101, doi:10.1029/91JA02697.

Anderson, B. J., et al. (1996), Source region of 0.2 to 1.0 Hz geomagnetic pulsation bursts, *Geophys. Res. Lett.*, *23*(7), 769–772, doi:10.1029/96GL00659.

Bortnik, J., et al. (2007), An automatic wave detection algorithm applied to Pc1 pulsations, *J. Geophys. Res.*, *112*, A04204, doi:10.1029/2006JA011900.

Bortnik, J., et al. (2008), Characteristics of low-latitude Pc1 pulsations during geomagnetic storms, *J. Geophys. Res.*, *113*, A04201, doi:10.1029/2007JA012867.

Chen, L., et al. (2009), Simulation of EMIC wave excitation in a model magnetosphere including structured high-density plumes, *J. Geophys. Res.*, *114*, A07221, doi:10.1029/2009JA014204.

Cornwall, J. M. (1965), Cyclotron instabilities and electromagnetic emissions in the ultra low frequency and very low frequency ranges, *J. Geophys. Res.*, *70*, 61–69.

Darrouzet, F., et al. (2009), Plasmaspheric density structures and dynamics: Properties observed by the CLUSTER and IMAGE missions, *Space Sci. Rev.*, 145(1/2), 55–106, doi:10.1007/s11214-008-9438-9.

Darrouzet, F., et al. (2013), Links between the plasmapause and the radiation belt boundaries as observed by the instruments CIS, RAPID and WHISPER onboard Cluster, *J. Geophys. ResSpace Physics*, *118*, 4176–4188, doi:10.1002/jgra.50239.

Décréau, P. M. E., et al. (2001), Early results from the Whisper instrument on Cluster: An overview, *Ann. Geophys.*, *19*(10/12), 1241–1258, doi:10.5194/angeo-19-1241-2001.

Denton, R. E., et al. (2002), Location of Pc 1–2 waves relative to the magnetopause, *Ann. Geophys.*, *20*, 1763–1767, doi:10.5194/angeo-20-1763-2002.

Engebretson, M. J., et al. (2008a), Temporal and spatial characteristics of Pc1 waves observed by ST5, *J. Geophys. Res.*, *113*, A07206, doi:10.1029/2008JA013145.

Engebretson, M. J., et al. (2008b), Pc1–Pc2 waves and energetic particle precipitation during and after magnetic storms: Superposed epoch analysis and case studies, *J. Geophys. Res.*, *113*, A01211, doi:10.1029/2007JA012362.

Fraser, B. J. (1975), Ionospheric duct propagation and Pc 1 pulsation sources, *J. Geophys. Res*., *80*(19), 2790–2796, doi:10.1029/JA080i019p02790.

Fraser, B. J. (1985), Observations of ion cyclotron waves near synchronous orbit and on the ground, *Space Sci. Rev.*, *42*, 357–374.

Fraser, B. J., and T. S. Nguyen (2001), Is the plasmapause preferred source region of electromagnetic ion cyclotron waves in the magnetosphere? *J. Atm. Solar-Terr. Phys.*, *63*, 1225–1247.

Fraser, B. J., et al. (2010), Storm time observations of electromagnetic ion cyclotron waves at geosynchronous orbit: GOES results, *J. Geophys. Res.*, *115*, A05208, doi:10.1029/2009JA014516.

Fukunishi, H., et al. (1981), Classification of hydromagnetic emissions based on frequency-time spectra, *J. Geophys. Res.*, *86*(A11), 9029–9039, doi:10.1029/JA086iA11p09029.

Gendrin, R., (1975), Is the plasmapause a preferential region for proton precipitation? *Ann. Geophys.*, *31*, 127.

Greifinger, C., and P. S. Greifinger (1968), Theory of hydromagnetic propagation in the ionospheric waveguide, *J. Geophys. Res.*, *73*(23), 7473–7490, doi:10.1029/JA073i023p07473.

Hayashi, K., et al. (1981), The extent of Pc 1 source region in high latitudes, *Can. J. Phys.*, *59*(8), 1097–1105, doi:10.1139/p81–145.

Horne, R. B., and R. M. Thorne (1993), On the preferred source location for the convective amplification of ion cyclotron waves, *J. Geophys. Res.*, *98*(A6), 9233–9247, doi:10.1029/92JA02972.

Horne, R. B., and R. M. Thorne (1997), Wave heating of He+ by electromagnetic ion cyclotron waves in the magnetosphere: Heating near the H+-He+ bi-ion resonance frequency, *J. Geophys. Res.*, *102*(A6), 11457–11471, doi:10.1029/97JA00749.

Johnson, J. R., and C. Z. Cheng (1999), Can ion cyclotron waves propagate to the ground? *Geophys. Res. Lett.*, *26*(6), 671– 674, doi:10.1029/1999GL900074.

Keika, K., et al. (2013), Global characteristics of electromagnetic ion cyclotron waves: Occurrence rate and its storm dependence, *J. Geophys. Res. Space Physics*, *118*, 4135–4150, doi:10.1002/jgra.50385.

Kersten, T., et al. (2014), Electron losses from the radiation belts caused by EMIC waves, *J. Geophys. Res. Space Physics*, *119*, doi:10.1002/2014JA020366.

Kerttula, R., et al. (2001), Storm-time Pc1 activity at high and middle latitudes, *J. Geophys. Res.*, *106*(A4), 6213–6227, doi:10.1029/2000JA900125.

Kim, H., et al. (2011), Statistical study of Pc1–2 wave propagation characteristics in the high-latitude ionospheric waveguide, *J. Geophys. Res.*, *116*, A07227, doi:10.1029/2010JA016355.

Kozyra, J. U., et al. (1984), Effects of energetic heavy ions on electromagnetic ion cyclotron wave generation in the plasmapause region, *J. Geophys. Res.*, *89*(A4), 2217–2233, doi:10.1029/JA089iA04p02217.

Liu, Y. H., B. J. Fraser, and F. W. Menk (2012), Pc2 EMIC waves generated high off the equator in the dayside outer magnetosphere, *Geophys. Res. Lett.*, *39*, L17102, doi:10.1029/2012GL053082.

Liu, Y. H., et al. (2013), EMIC waves observed by Cluster near the plasmapause, *J. Geophys. Res. Space Physics*, *118*, 5603–5615, doi:10.1002/jgra.50486.

Loto'aniu, T. M., et al. (2005), Propagation of electromagnetic ion cyclotron wave energy in the magnetosphere, *J. Geophys. Res.*, *110*, A07214, doi:10.1029/2004JA010816.

Manchester, R. N. (1970), Propagation of hydromagnetic emissions in the ionospheric duct, *Planet. Space Sci.*, *18*, 299–307, doi:10.1016/0032-0633(70)90166-2.

Mann, I. R., et al. (2008), The Upgraded CARISMA Magnetometer Array in the THEMIS Era, *Space Sci. Rev.*, *141*: 413–451, doi: 10.1007/s11214-008-9457-6.

Mann, I. R., et al. (2014), Spatial localization and ducting of EMIC waves: Van Allen Probes and ground-based observations, *Geophys. Res. Lett.*, *41*, 785–792, doi:10.1002/2013GL058581.

Mauk, B. H. (1982), Helium resonance and dispersion effects on geostationary Alfvén/ion cyclotron waves, *J. Geophys. Res.*, *87*(A11), 9107–9119, doi:10.1029/JA087iA11p09107.

Meredith, N. P., et al. (2014), Global morphology and spectral properties of EMIC waves derived from CRRES observations, *J. Geophys. Res. Space Physics*, *119*, 5328–5342, doi:10.1002/2014JA020064.

McCollough, J. P., S. R. Elkington, M. E. Usanova, I. R. Mann, D. N. Baker, and Z. C. Kale (2010), Physical mechanisms of compressional EMIC wave growth, *J. Geophys. Res.*, *115*, A10214, doi:10.1029/2010JA015393.

Miyoshi, Y., et al. (2008), Precipitation of radiation belt electrons by EMIC waves, observed from ground and space, *Geophys. Res. Lett.*, *35*, L23101, doi:10.1029/2008GL035727.

Perraut, S., et al. (1984), Ion cyclotron waves: Direct comparison between ground-based measurements and observations in the source region, *J. Geophys. Res.*, *89*(A1), 195–202, doi:10.1029/JA089iA01p00195.

Posch, J. L., M. J. Engebretson, M. T. Murphy, M. H. Denton, M. R. Lessard, and R. B. Horne (2010), Probing the relationship between electromagnetic ion cyclotron waves and plasmaspheric plumes near geosynchronous orbit, *J. Geophys. Res.*, *115*, A11205, doi:10.1029/2010JA015446.

Prikner, K., et al. (2004), An effect of the ionospheric Alfvén resonator on multiband Pc1 pulsations, *Ann. Geophys.*, *22*, 643–651, doi:10.5194/angeo-22-643-2004.

Rauch, J. L., and A. Roux (1982), Ray tracing of ULF waves in a multicomponent magnetospheric plasma: Consequences for the generation mechanism of ion cyclotron waves, *J. Geophys. Res.*, *87*(A10), 8191–8198, doi:10.1029/JA087iA10p08191.

Reeves, G. D. (2007), Radiation belt storm probes: A new mission for space weather forecasting. *Space Weather*, *5*: n/a. doi: 10.1029/2007SW000341.

Roux, C., et al. (1982), Wave-particle interaction near He+ observed on board GEOS 1 and 2: 2. Generation of ion cyclotron waves and heating of He+ ions, *J. Geophys. Res.*, *87*, 8174–8190, doi:10.1029/JA087iA10p08174.

Sakaguchi, K., et al. (2013), Akebono observations of EMIC waves in the slot region of the radiation belts, *Geophys. Res. Lett.*, *40*, 5587–5591, doi:10.1002/2013GL058258.

Silin, I., et al. (2011), Warm plasma effects on electromagnetic ion cyclotron wave MeV electron interactions in the magnetosphere, *J. Geophys. Res.*, *116*, A05215, doi:10.1029/2010JA016398.

Søraas F., et al. (1980), A comparison between simultaneous IPDP ground-based observations and observations of energetic protons obtained by satellites, *Planet. Space Sci.*, *28*(4), 387–405.

de Soria-Santacruz, M., M. Spasojevic, and L. Chen (2013), EMIC waves growth and guiding in the presence of cold plasma density irregularities, *Geophys. Res. Lett.*, *40*, 1940–1944, doi:10.1002/grl.50484.

Summers, D., et al. (1998), Relativistic theory of wave-particle resonant diffusion with application to electron acceleration in the magnetosphere, *J. Geophys. Res.*, *103*(A9), 20487–20500, doi:10.1029/98JA01740.

Summers, D., and R. M. Thorne (2003), Relativistic electron pitch-angle scattering by electromagnetic ion cyclotron waves during geomagnetic storms, *J. Geophys. Res.*, *108*, 1143, doi:10.1029/2002JA009489, A4.

Thorne, R. M., et al. (2006), Interaction of EMIC waves with thermal plasma and radiation belt particles, in *Magnetospheric ULF Waves: Synthesis and New Directions* (eds. K. Takahashi, P. J. Chi, R. E. Denton, and R. L. Lysak), AGU, Washington, DC, doi:10.1029/169GM14

Turner, D. L., et al. (2013), On the storm-time evolution of relativistic electron phase space density in Earth's outer radiation belt, *J. Geophys. Res. Space Physics*, *118*, 2196–2212, doi:10.1002/jgra.50151.

Ukhorskiy, A. Y., et al. (2010), Rapid scattering of radiation belt electrons by storm-time EMIC waves, *Geophys. Res. Lett.*, *37*, L09101, doi:10.1029/2010GL042906.

Usanova, M. E., et al. (2008), Multipoint observations of magnetospheric compression-related EMIC Pc1 waves by THEMIS and CARISMA, *Geophys. Res. Lett.*, *35*, L17S25, doi:10.1029/2008GL034458.

Usanova, M. E., et al. (2010), Conjugate ground and multisatellite observations of compression-related EMIC Pc1 waves and associated proton precipitation, *J. Geophys. Res.*, *115*, A07208, doi:10.1029/2009JA014935.

Usanova, M. E., et al. (2012), THEMIS observations of electromagnetic ion cyclotron wave occurrence: Dependence on AE,

SYMH, and solar wind dynamic pressure, *J. Geophys. Res.*, *117*, A10218, doi:10.1029/2012JA018049.

Usanova, M. E., et al. (2013), Statistical analysis of EMIC waves in plasmaspheric plumes from Cluster observations, *J. Geophys. Res. Space Physics*, *118*, 4946–4951, doi:10.1002/jgra.50464.

Usanova, M. E., et al. (2014), Effect of EMIC waves on relativistic and ultra-relativistic electron populations: Ground-based and Van Allen Probes observations, *Geophys. Res. Lett.*, *41*, doi:10.1002/2013GL059024.

Woodroffe, J. R., and R. L. Lysak (2012), Ultra-low frequency wave coupling in the ionospheric Alfvén resonator: Characteristics and implications for the interpretation of ground magnetic fields, *J. Geophys. Res.*, *117*, A03223, doi:10.1029/2011JA017057.